The effect of substrate pre-treatment on durability of rubber-stainless steel adhesion

E. Sarlin[1], M. Honkanen[2], M. Lindgren[3], P. Laihonen[3], M. Juutilainen[4], M. Vippola[1,2], J. Vuorinen[1]

[1]Tampere University, Engineering Materials Science, P.O. Box 589, 33014 Tampere University, Finland

[2]Tampere University, Tampere Microscopy Center, P.O. Box 692, 33014 Tampere University, Finland

[3]Outotec Research Center, Kuparitie 10, 28330 Pori, Finland

[4]Teknikum Oy, P.O. Box 13, 38210 Sastamala, Finland

Corresponding author: essi.sarlin@tuni.fi, +358 40 849 0146

Surfaces and Interfaces Volume 21, December 2020, 100646

https://doi.org/10.1016/j.surfin.2020.100646

ABSTRACT

In many applications, rubber linings protect metal surfaces from the environment and prolong the service life of the metal components significantly. The loss of adhesion and resulting premature failure at the rubber-metal interface may generate an un-planned shutdown and production losses. This work focuses on the effect of various sand blasting methods on the long-term adhesion between bromobutyl rubber and stainless steel in a hot and humid environment. Softer austenitic stainless steel and harder, chemically more resistant super duplex stainless steel grades were used as substrates. It was found, that the developed interfacial area ratio S_{dr}, which is the additional surface area contributed by the texture as compared to the planar definition area, had the best correlation with the sand blasting media

characteristics, namely to the hardness. The proportionality between other sand blasting medium characteristics and the S_{dr} value was poor. The initial adhesion between the rubber and the substrates was defined by the cohesive strength of the rubber and unaffected by the substrate characteristics and the sand blasting medium contaminants on the substrates. After a 4-12-week exposure in hot and humid environment, the use of corrosive sand blasting medium (steel grit) resulted in significant adhesion loss whereas the use of inert sand blasting media (feldspar or corundum) maintained the adhesion better. However, the adhesion system at the interface degraded causing performance loss. Neither the better corrosion resistance of super duplex stainless steel nor increased surface roughness improved the reliability of rubber lining in extreme conditions.

Keywords: Steel-rubber adhesion; Sand blasting; Surface roughness; Ageing

1. INTRODUCTION

Rubber linings protect metal surfaces from wear and chemical attack and prolong the service life of the metal components significantly. Ideally, the maintenance interval of the rubber lining is defined by the wear or degradation rate of the rubber in the service environment. These factors are typically relatively well known which makes the optimization of the rubber lining design and its lifetime prediction straightforward. However, in an alternative scenario the loss of adhesion and the premature failure at the rubber-metal interface generates an un-planned shutdown that typically leads to significant production losses. Thus, to ensure the structural integrity of rubber-lined components, it is crucial to understand all the factors that affect the durability of rubber-metal adhesion.

The most straightforward way to attach rubber linings to metal surfaces is so called vulcanisation bonding process. In the process, the adhesive system between the metal surface and the rubber is cured during the vulcanization of the rubber. The surface treatment of the metal substrate plays a major role in the initial adhesion level and its durability. Surface cleaning and descaling with alkaline or acidic solutions are the minimum requirements but increasing the surface roughness is a standard procedure as well. Sand blasting is argued to be time-consuming and the resulting surface characteristics are uncontrolled [1, 2]. Alternatives can be found from more advanced methods, such as electrochemical treatments, plasma-assisted methods and laser-based precision processing methods [1, 3]. However, these methods have not replaced sand blasting in the industry as sand blasting is often easily available and does not require expensive equipment.

The studies on the sand blasted surfaces have focused on the roughness introduced by the treatment. Typically, the increased substrate surface roughness is reported to improve the adhesion up to some case specific optimum value [e.g. 2, 4]. Also, the shape of the substrate

surface irregularities has been studied and regular geometries have been found to be the most effective on improving the adhesion [5]. From this point of view, sand blasting treatments are not favoured, as it is not possible to control the micro-geometry of a sand blasted surface [2]. The surface roughness of the substrate is traditionally described by 2D parameters, most often the R_a value, but modern profilometers have allowed the use of 3D parameters, the "S" values. The S value can contain data about the height of the surface features, their frequency, or both.

As a standard procedure, the sand blasted surfaces are cleaned and only a few studies discuss the effect of possible residues of sand blasting medium on adhesion. Day et al. [6] have formulated an equation to evaluate the grit contamination of the substrate but its confidence level was shown to be poor. In addition, they did not study the effect of grit material properties apart from grit size. Poon et al. [7] have characterized structural steel surface after sand blasting with almandine or steel grit. They found that the amount of sand blasting medium residues was stabilized after 10 s sand blasting time and was independent on the sand blast gun pressure. The residues were not removable by different cleaning methods including air jet, rinsing or sonication. Poon et al. [7] also concluded that the sand blasting medium residues might compromise the adhesion between the steel substrate and an organic coating. As an alternative to the traditional sand blasting media, such as metal grits or different minerals (sand), dry ice can be used [8] to avoid the residues but it also introduces the specific equipment requirements for the surface treatment process.

The focus of this study is the effect of various sand blasting methods on the long-term adhesion between bromobutyl rubber and stainless steel in a hot and humid environment. Two stainless steel grades with varying hardness were sand blasted with different media, namely steel grit, feldspar and corundum. The resulting surfaces were thoroughly characterized and

the surface properties are discussed in respect to the measured peel strength and its long-term behaviour.

2. MATERIALS AND METHODS

2.1 Materials

Completely bromobutyl rubber (BIIR) encapsulated metal inserts were prepared from an austenitic stainless steel (denoted as SS, grade EN 1.4432/316L) and super duplex stainless steel (denoted as SD, grade EN 1.4410/2507). The super duplex stainless steels contain approximately equal amounts of austenite and ferrite phases. The stainless steel 1.4432 is used in highly corrosive environments whereas the super duplex stainless steel 1.4410 has even higher corrosion resistance, higher strength and enhanced resistance to stress corrosion cracking than the austenitic stainless steel grade 1.4432. The hardness of the austenitic stainless steel is 170 HV3 and the super duplex stainless steel is 310 HV3. The initial surface roughness R_a values were 0.3 µm for SS and 2.2 µm for SD.

The metal inserts (sized 25 x 60 x 3 mm) were sand blasted in an industrial environment to improve the adhesion by cleaning and increasing the roughness of the surfaces. The sand blasting pressure was 7 bar for all sand blasting media. The properties of the sand blasting media are listed in Table I and the micrographs are shown in Figure 1. The steel grit was a mixture of two different grit sizes: 50% 0.4-1.2 mm and 50% 0.2-0.7 mm. The shape of all sand blasting media was irregular (angular grit) and, therefore, the effect of the particle shape should be rather similar in all of the cases. In general, the hardness of abrasive particles cannot be directly related to the amount of abrasive material residues on the sand blasted surface [9], as the resulting surface characteristics depend also on the sand blasting process parameters, abrasive particle size and shape and the substrate. Smaller abrasive sizes have shown to lead to higher contamination of the surface [9].

2.2 Steel surface characterization

The sand blasted stainless steel surfaces were studied with a scanning electron microscope (SEM, Zeiss ULTRAplus, Germany) equipped with an energy dispersive X-ray spectroscopy detector (EDS, INCA Energy analysator with INCAx-act silicon-drift detector, SDD, Oxford Instruments, UK) and an Electron Backscatter Diffraction (EBSD system, Symmetry, Oxford Instruments, UK). A step size of 0.3 or 0.5 µm and an acceleration voltage of 20 kV were used. For SEM/EDS studies, no additional sample preparation was required. The cross-sectional EBSD samples were sectioned, ground and polished followed by a final polishing using colloidal silica suspension (0.04 µm). The steel surfaces were also studied with an optical profilometer system (Alicona InfiniteFocus G5 3D profilometer, Austria) to measure the surface roughness after the surface treatments.

2.3 Hybrid material preparation and characterization

To achieve required adhesion between the rubber and the steel, a commercial bromobutyl based adhesive treatment from REMA TIP TOP was used. The adhesive system included two primers (PR500-1 and S500-2) and an adhesive (TC5000), applied in this order on the metal surface. To prepare the peel test samples, the adhesive was applied only to the central area (25 mm x 25 mm) of the metal inserts and no adhesion or very weak one was formed elsewhere. After the adhesive treatment, the metal inserts were covered with a 5 mm thick BIIR layer from both sides and the samples were vulcanized which also induced the curing of the adhesive system. The sample preparation is schematically illustrated in Figure 2.

The encapsulation of the metal inserts with rubber ensured that no molecule transport along the interface and resultant fast interfacial degradation could occur. The degradation of the interfacial adhesion had to be induced by increased temperature and/or molecules diffused

from the surrounding environment through the rubber to the interface, as it is also the case in the actual service environment of metal parts with rubber lining.

The samples were aged in water immersion at 95 ºC. In our previous study [10], it was demonstrated that for hot and chemically aggressive environments, e.g. acidic environments, ageing in pure deionized water led to similar or conservative results. Here, the duration of the ageing was 4 or 12 weeks. The interfacial strength was tested with 90º peel test at a crosshead rate of 50 mm/min according to the ISO-813:1997 (E) [11]. A universal testing machine Instron 5967 with a 30 kN load cell was used. Prior the peel testing, the samples were opened with a Stanley knife and the excess rubber was removed around the steel inserts (see Figure 2, steps 5-6). The maximum peel force was taken to calculate the peel strength. At least two samples for each sample type (combination of specific substrate material and sand blasting medium) and ageing condition were tested.

After the peel tests the metal inserts were studied with SEM and EDS without any additional sample preparation steps. The area fraction of the cohesive fracture in the peel test samples was estimated from photographs of the metal inserts after peel testing by image analysis software (ImageJ). The fracture location in the large scale studies could be classified into only two categories: “cohesive” referring to a fracture location in the adhesive system or in the rubber and “adhesive” referring to a failure at the steel-primer interface. This was due to the similar colour and composition of the primers, adhesive and the rubber. More detailed classification of fracture locations would have been possible from the cross-sectional focused ion beam SEM (FIB-SEM) samples but as this method is not suitable for large scale studies, it was not used to estimate the overall fractions of fracture location.

To investigate the cross-section of the rubber-metal interface, samples were also examined with a FIB-SEM (Zeiss Crossbeam 540, Germany) equipped with EDS ($XMax^N$ SDD, Oxford Instruments, UK). The cross-sections of the peeled samples (metal inserts) before and after ageing were prepared by depositing a platinum (Pt) protection layer on the region of interest and using gallium (Ga) ions to mill the cross-section under the Pt covering layer. Prior to the FIB-SEM studies, the samples were gold-coated to avoid the sample charging during the milling process.

3. RESULTS AND DISCUSION

3.1 Metal surface characterization after sand *blasting*

Figure 3 presents the EDS and SEM images of the sand blasted surfaces. The shape of the surface irregularities was rather similar in all cases as it was expected due to the similar shapes of the sand blasting media. Although the sand blasting process was finalized with cleaning the surfaces with blast air, following the standard procedure in the industry, all surfaces exhibited residues from the sand blasting media, which is visible from the EDS phase maps as white areas. The sand blasting medium phase maps from stainless steel and super duplex stainless steel surfaces were very similar. In the SEM images (the right-hand side of Figure 3.b-d), the residues are visible as whiteish areas (indicated with arrows). However, in the case of the steel grit treated surfaces (Figure 3.a), the residues have similar average atomic weight to the substrate are therefore not visible due to the contrast formation mechanism of SEM. In the literature, 1-50% abrasive particle embedment of metal surfaces after sand blast cleaning have been reported [9].

The EBSD measurements are a vehicle to study plastic deformation of the austenitic stainless steel (austenite with face centred cubic (fcc) crystal structure) and the super duplex stainless steel (both austenite with fcc crystal structure and ferrite with body centred cubic (bcc) crystal

structure) surfaces after sand blasting by corundum C20. In the EBSD results, a band contrast (BC) map represents the quality of the Kikuchi diffraction pattern for each measurement pixel. In the BC map, bright signifies that the pattern quality is good, it can be indexed, and crystal orientation can be determined. Black signifies that the pattern quality is poor. The colours in the inverse pole figure (IPF) maps (Z direction) correspond to the crystallographic orientations parallel to the observed plane as indicated by the coloured stereographic triangle, i.e. an IPF colouring key. Phase maps show the distribution of austenite, ferrite, and corundum.

The EBSD results for the austenitic stainless steel before and after the sand blasting by corundum are presented in Figure 4. Before the sand blasting (Figure 4.a), indexing austenite structure succeeded very well. Based on the results, plastic deformation has occurred on the sand blasted surface (Figure 4.b), i.e. indexing the austenite structure was not successful on the 50-100 µm distance from the steel surface. According to the phase map, corundum residues exist on the sand blasted steel surface.

The EBSD results for the super duplex stainless steel (Figure 5) indicate that plastic deformation has occurred on the 50 µm distance from the surface and the deformed surface layer was somewhat thinner than in the austenitic stainless steel sample. The higher hardness of the super duplex stainless steel that arises from the ferrite phase, seems to protect the surface from plastic deformation during the sand blasting compared to the softer austenitic stainless steel. The austenite and the ferrite phases in the super duplex material have different mechanical properties [12] and hardness but the plastic deformation induced by the sand blasting seem to have spread equally to both phases. The sand blasting medium seems to have attached both to the harder and softer stainless steel surfaces. Industrial standard procedure to

clean the sand blasted surface (pressurized air) is clearly not enough to prevent the contamination of the surface.

The three different sand blasting media varied in terms of composition, hardness and size (see Table I) and our assumption was that these factors have an effect on the resulting surface properties of the stainless steels. The surface roughness measurement results for both steel grades after different surface treatments are shown in Table II and Figure 6. For the austenitic stainless steel, there was a trend of increasing arithmetic mean roughness value S_a with increasing sand blasting medium hardness (Figure 6.a), whereas for super duplex stainless steel there was no identifiable correlation. In a previous study, the as received super duplex stainless steel surface was found to exhibit some waviness due to its production method, whereas the stainless steel surface was found to be very flat [13]. The possible effect of waviness on the surface roughness values (S_a or S_{dr}) could not be identified and compensated from the results although it is considered to be the reason for the higher roughness values of the harder substrate. Thus, the analysis of the effect of sand blasting media on the surface roughness for the austenitic stainless steel is considered more reliable in this case. Arithmetic mean roughness value S_a is the typical parameter to evaluate the surface roughness of machined surfaces and it represents an average measure of the surface texture. However, it is insensitive in differentiating peaks, valleys and the spacing of the various texture features and thus fails to describe the surface unambiguously. Therefore, dissimilar surfaces in terms of spatial and height symmetry features can have similar S_a values and the suitability of S_a values to describe surface roughness is generally criticised.

Developed interfacial area ratio S_{dr}, which is the additional surface area contributed by the texture as compared to the planar definition area, is considered to be more sensitive to surface morphology (surface feature amplitude and spacing) and describe better the adhesion

behaviour of a surface than S_a [14]. However, similar to S_a it does not take into account the shape (e.g. roundness or symmetry) of the surface features, which can have an effect on the mechanical interlocking at the interface. The S_{dr} results were virtually the same for both steel grades. Additionally, there was a clear trend for both substrates relating increasing surface roughness to increasing media hardness (Figure 6.b). Naturally, harder particles cause deeper surface profile, i.e. rougher surface finish. The trend was slightly clearer for the austenitic stainless steel than for the super duplex stainless steel, which can be expected due to its softer surface. Other reasons for this difference could be the anisotropic shape of the austenite and ferrite phases and the differences in the mechanical behaviour of the phases [12].

Day et al. [6] have shown a linear equation for the surface roughness (maximum height of the profile R_z) as a function of grit size and sand blast process parameters with a very good confidence level. They reported the coefficient of -3.5 for the grit size in the case of Al_2O_3 predicting decreasing roughness with increasing grit size. If the S_a or S_{dr} values measured for the SS and SD surfaces are compared with the abrasive particle diameter (D50 value), the correlation is poor even within the same hardness abrasive particles (corundum). Based on kinetic energy consideration ($E_{kin}=½mv^2$) one would expect sand blasting with larger particles to generate higher surface roughness. In erosion and erosion-corrosion studies [15] it has, however, been noticed that particle size had less effect than the energy consideration predicted. The reason for this type of behaviour can be related to the particle shape, brittleness and number per area. It has been reported that only small cutting edges of the particles are in contact with the target material [16] and the size of the cutting edges and angular corners can be rather insensitive to particle size. The effect may be enhanced if the particles are brittle and fracture easily while colliding with each other causing changes to the size and shape of the particles that actually impinge to the target surface. Also, use of larger abrasive particles lead to lower number of particles colliding to a specific area [9].

3.2 Rubber metal adhesion

The peel test force results are defined by the properties of the interface and the properties of the peeled material, i.e. rubber. In this study, we assumed that the properties of the steel inserts did not change, and that the adhesion system and the rubber layer were similar in all samples. Thus, the only variables were the surface properties of the steel substrate. If a peel test reveals an adhesive failure, the behaviour of the structure can be regarded as less reliable in the actual service than if the fracture location would be cohesive inside one of the components. This is because the cohesive properties of materials are typically far better known than the interfacial properties and are therefore more predictable. Thus, a cohesive failure was considered as a positive outcome in this study.

The initial peel tests resulted in purely cohesive fracture inside rubber with an average peel strength of 10.4 ± 0.4 N/mm^2 for all surface finishes. Thus, the sand blasting medium contamination of the substrates did not compromise the initial adhesion despite its significant surface coverage (Figure 3). Similarly, the variation in the surface roughness did not yield to differences in the measured initial peel strength. The adhesive system at the interface together with the surface roughness provides an interfacial strength that exceeds the cohesive strength of the rubber.

In the presence of water, steel grit (composition C 0.80-1.20%, Mn 0.60-1.20%, Si $\geq$ 0.40%, S and P $\leq$ 0.05%, Fe balance; defined by the supplier) is prone to formation of iron oxides (corrosion). Under the hot-moist conditions used in this study, the volumetric changes accompanied with the oxidation of steel grit can cause disconnection of the rubber from the steel. In our previous study [10], it was observed in SEM studies that the feldspar residues are forced to the asperities of the steel surface and are well attached to the substrate but are not

detrimental to steel-rubber adhesion. Like the feldspar (solid solution of $NaAlSi_3O_8$, KSi_3O_8 and $CaAl_2Si_2O_8$), corundum (Al_2O_3 >99% purity according to the supplier) is inert in hot water and any volumetric changes of sand blasting medium residues at the rubber-stainless steel interface are not expected.

The peel test results after 4 and 12 week water immersion at 95 °C are shown in Figure 7. The steel grit treated samples for both stainless steel grades showed poorest performance both in terms of peel strength and fracture location even after 4 week immersion. The low peel strength values, adhesive fracture location and considerably low deviation of both results highlight that the interface between the steel substrates and the adhesive system has been very weak after ageing. Clearly the corrosion and the accompanied volume increase of the steel grit residues at the steel substrates caused failure to the steel-primer interface and deteriorated the initial bond. The use of steel grit as a sand blasting media is favoured if effective cleaning and high recyclability for the medium is required, but according to these results we do not recommended its use in hot/moist environments in which moisture can diffuse to the interface through the rubber lining.

Feldspar and both corundum samples resulted in rather similar long-term properties in aggressive environment. Significant differences in the effect of the sand blasting medium chemistry (feldspar vs. corundum C20) or grit size (corundum C20 vs. C24) could not be identified. Especially after the shorter immersion time, the scatter of the results was high (Figure 7). Naturally, higher number of samples could have reduced the deviation, but the fracture location results indicate that at the moment of testing (4 weeks immersion), the degradation rate of the adhesive system was high leading to highly scattered results. The samples in which the adhesive system was still active, the fracture location was cohesive and the peel strength closer to the initial value, whereas in other samples the deterioration of

adhesive system had proceeded further leading to more adhesive failure. During the longer immersion time, the degradation of the adhesive system can be assumed to stabilize leading to lower scatter values, mostly adhesive fracture and almost purely surface roughness dominated peel strength results. This kind of behaviour was observed for both austenitic stainless steel and super duplex stainless steel samples. For the austenitic stainless steel, increasing roughness (S_a or S_{dr} value) indicated improved performance in terms of higher peel strength and increased fraction of cohesive fracture (Figure 8). The relation became stronger after longer immersion time, as expected, as the peel fracture becomes more adhesive and the interfacial strength is more controlled by mechanical interlocking of rubber to the metal surface. The S_a value corresponded slightly better to the performance when compared to the S_{dr} values, but the differences were rather minimal. For super duplex stainless steel, any consistent trend between the peel strength or fracture location and the S_a or S_{dr} values could not be found. This is supposed to be due to the uncertainties in the surface roughness indicators due to the initial waviness of the surface. Neither the better corrosion resistance nor the higher hardness of the super duplex stainless steel improves the reliability of rubber lining.

To study the fracture location at the interface in more detail, cross-sections prepared by FIB-SEM were analysed along with profilometer results (Figure 9). Similar to our previous study [10], it was found that those areas, defined in the macroscopic fracture location analysis to be “cohesive”, where actually a variety of fracture locations inside the primer, adhesive and rubber. However, the porous structure of the adhesive and the primer, not present prior ageing, indicated that the adhesive system is the weak point of the structure in this environment. This explains also the similarity of the corundum and feldspar treated surfaces, as it is not the sand blasting medium contaminants or the changes in the ability of the rubber to mechanically interlock to the substrate that causes the decrease in the adhesion. Therefore,

it can also be concluded, that there is no need to optimize the adhesive system to fit both the metal surface and sand blasting medium chemistry, but the environmental resistance of the adhesive is the most important aspect.

5. CONCLUSIONS

In this work, we studied the effect of various sand blasting methods on the long-term adhesion between bromobutyl rubber and stainless steel in a hot and humid environment. Austenitic stainless steel and austenitic/ferritic super duplex stainless steel grades were sand blasted with corrosive and corrosion resistant media. Regardless on the substrate hardness or the abrasive particle material, the substrates were contaminated with abrasive material. The resulting surface roughness (especially S_{dr} rather than S_a) had a clear correlation between abrasive material hardness but not with its grit size. The initial adhesion between the rubber and the substrates was defined by the cohesive strength of the rubber and unaffected by the substrate characteristics and the sand blasting medium contaminants on the substrates. After the exposure to hot and humid environment, the substrates treated with corrosion resistant abrasive particles (feldspar and corundum) outperformed the corrosive steel grit blasted surface. However, the hot-moist environment caused adhesive system to fail regardless on the significant sand blasting medium contamination on the substrate. A trend of increasing adhesion resistance with increasing surface roughness was observed for the austenitic stainless steel. For the super duplex stainless steel the trend was absent, probably due to the initial waviness of the surface and resulting uncertainties in the surface roughness indicators. Neither the better corrosion resistance of super duplex stainless steel nor increased surface roughness improved the reliability of rubber lining in extreme conditions.

Acknowledgements

The work has been done within the FIMECC HYBRIDS program funded by Finnish Funding Agency for Technology (Tekes) and the participating companies. Mikko Esko, Kauko Östman, Anne Tauriainen, Meri Kiviniemi and Pasi Seppälä are gratefully acknowledged for their help with the experiments. Electron microscopy work made use of Tampere Microscopy Center facilities at Tampere University.

REFERENCES

[1]: B. Huang, L. Sun, L. Lijun, L. Zhang, Y. Lin, J. Che, Experimental investigation of the strength of polymer-steel direct adhesion (PSDA) joints with micro-structures ablated by laser, J. Mater. Process. Tech. 249 (2017) 407-414. https://doi.org/10.1016/j.jmatprotec.2017.06.031

[2]: E. Sancaktar, R. Gomatam, A study on the effects of surface roughness on the strength of single lap joints, J. Adhes. Sci. Technol. 15:1 (2001) 97-117. https://doi.org/10.1163/156856101743346

[3]: A. Latifi, M. Imanib, M. T. Khorasanic, M. D. Joupari, Plasma surface oxidation of 316L stainless steel for improving adhesion strength of silicone rubber coating to metal substrate, Appl. Surf. Sci. 320 (2014) 471–481. http://dx.doi.org/10.1016/j.apsusc.2014.09.084

[4]: D. Pradhan, R. Ghosh, A. Banerjee, M. Dutta, Effect of electro-cleaning roughness on steel wire-rubber adhesion strength, Surf. Coat. Tech. 286 (2016) 293–302. http://dx.doi.org/10.1016/j.surfcoat.2015.12.048

[5]: L. Shen, L. Sun, L. Li, B. Huang, X. Ye, The effect of interfacial microstructures on joining strength of polymer-metal hybrid interface, Proceedings of the ASME 2016 International Mechanical Engineering Congress and Exposition, Volume 14: Emerging Technologies; Materials: Genetics to Structures; Safety Engineering and Risk Analysis. Phoenix, Arizona, USA. November 11–17, 2016. https://doi.org/10.1115/IMECE2016-65811

[6]: J. Day, X. Huang, N.L. Richards, Examination of a grit-blasting process for thermal spraying using statistical methods, J. Therm. Spray. Techn. 14:4 (2005) 471-479. https://doi.org/10.1361/105996305X76469

[7]: J. Poon, D. C. Madden, M. H. Wood, S. M. Clarke, Characterizing surfaces of garnet and steel, and adsorption of organic additives, Langmuir 34:26 (2018) 7726-7737. https://doi.org/10.1021/acs.langmuir.8b01405

[8]: S. Dong, H. Liao, Substrate pre-treatment by dry-ice blasting and cold spraying of titanium, Surf. Eng. 34:3 (2018) 173-180. https://doi.org/10.1080/02670844.2016.1210894

[9]: A. Momber, Blast Cleaning Technology, Springer-Verlag Berlin Heidelberg, 2008.

[10]: E. Sarlin, A. Rosling, M. Honkanen, M. Lindgren, M. Juutilainen, M. Poikelispää, P. Laihonen, M. Vippola, J. Vuorinen, Effect of environment on bromobutyl rubber–steel adhesion, Rubber Chem. Technol. https://doi.org/10.5254/rct.19.80455

[11]: ISO 813 Standard: Rubber, vulcanized or thermoplastic — Determination of adhesion to a rigid substrate — 90 degree peel method, 1997.

[12]: J. J. Moverare, M. Odén, Deformation behaviour of a prestrained duplex stainless steel, Mater. Sci. Eng., A337 (2002) 25-38. https://doi.org/10.1016/S0921-5093(02)00022-9

[13]: M. Lindgren, R. Suihkonen, J. Vuorinen, Erosive wear of various stainless steel grades used as impeller blade materials in high temperature aqueous slurry, Wear 328-329 (2015) 391–400. https://doi.org/10.1016/j.wear.2015.03.014

[14]: R. K. Leach, Surface topography characterization, in: R. K. Leach (Edit.), Micro and Nano Technologies, Fundamental Principles of Engineering Nanometrology, William Andrew Publishing, Oxford, 2010, pp. 211-262.

[15]: M. Lindgren, S. Siljander, R. Suihkonen, P. Pohjanne, J. Vuorinen, Erosion-corrosion resistance of various stainless steel grades in high-temperature sulfuric acid solution, Wear, 364-365 (2016) 10-21. https://doi.org/10.1016/j.wear.2016.06.007

[16]: Z.G. Liu, S. Wan, V.B. Nguyen, Y.W. Zhang, A numerical study on the effect of particle shape on the erosion of ductile materials, Wear 313 (2014) 135-142. https://doi.org/10.1016/j.wear.2014.03.005

List of Tables and Table Captions

Table I: *The hardness of the blasting media provided by the material suppliers and the median diameter (D50) values measured by sieve analysis.*

Blasting medium	Denoting code	Mohs hardness [-]	D50 [µm]	Supplier
Steel grit	SG	≥ 5.5*	430	Beijer
Feldspar	F	6	930	Sibelco
Corundum F20	C20	9	1060	Beijer
Corundum F24	C24	9	750	Beijer

* The hardness of the steel grit defined by the supplier is ≥ 60 HRC

Table II: *The surface roughness results for the surface treated (see Table I) stainless steel (SS) and super duplex stainless steel (SD) steel: Average height of selected area S_a and developed interfacial area (S_{dr}).*

	SS_SG	SS_F	SS_C20	SS_C24	SD_SG	SD_F	SD_C20	SD_C24
S_a [µm]	11.9	20.3	18.3	32.4	30.2	20.9	27.0	28.7
S_{dr} [%]	9.6	9.8	22.0	23.0	9.9	6.5	20.0	17.7

List of Figure Captions

Figure 1: *Micrographs of the blasting media: a) steel grit, b) feldspar, c) corundum.*

Figure 2: *Schematic presentation of the sample preparation (1-3), ageing (4) and peel testing (5-6).*

Figure 3: *EDS phase maps for blasting media on austenitic stainless steel substrate (left) and higher magnification SEM micrographs (right) from the austenitic stainless steel (SS) and super duplex stainless steel (SD) surfaces after blasting with a) steel grit, b) feldspar, c) corundum C20 and d) corundum C24.*

Figure 4: *The inverse pole figure (IPF) map superimposed on the band contrast (BC) map collected from stainless steel a) before and b) after blasting by corundum C20. The colours in the IPF maps correspond to the orientations parallel to the observed plane as indicated by c) the IPF colouring key. After blasting by corundum, also the phase map superimposed on the BC map is presented, austenite is blue and corundum is yellow.*

Figure 5: *The inverse pole figure (IPF) map superimposed on the band contrast (BC) map collected from stainless steel a) before and b) after blasting by corundum C20. The colours in the IPF maps correspond to the orientations parallel to the observed plane as indicated by c) the IPF colouring key. After blasting by corundum, also the phase map superimposed on the BC map is presented, austenite is blue ferrite is red and corundum is yellow.*

Figure 6: *The correlation between the blasting medium hardness and a) the resulting steel surface height profile S_a and b) the developed interfacial area S_{dr}. The corundum type (see Table I) is indicated separately.*

Figure 7: *The average peel test results (a) and the location of the fracture (b) together with the standard deviation values. The reference values for the virgin samples were 10.4 N/mm^2 and 100% cohesive fracture for the peel strength and fraction of cohesive fracture, respectively.*

Figure 8: *The average peel strength versus a) the S_a value and b) the S_{dr} value.*

Figure 9: *The 3D image, height map, and optical image (collected by optical profilometer) from the same area together with cross-sectional FIB-SEM images after the peel test (the metal insert) of the super duplex based steel-rubber hybrid aged in deionized water at 95 °C for 12 weeks.*

1

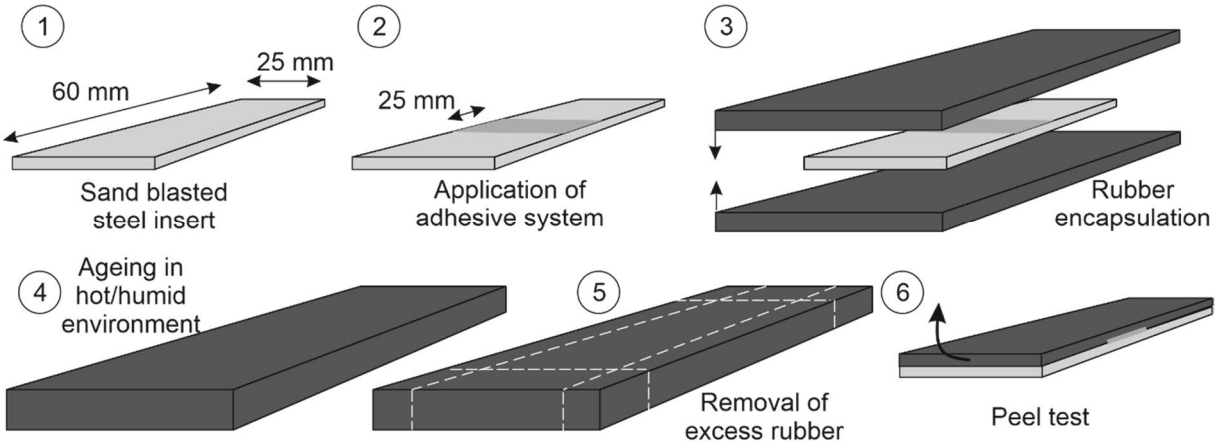
1
60 mm
25 mm
Sand blasted
steel insert
2
25 mm
Application of
adhesive system
3
Rubber
encapsulation
4
Ageing in
hot/humid
environment
5
Removal of
excess rubber
6
Peel test

2

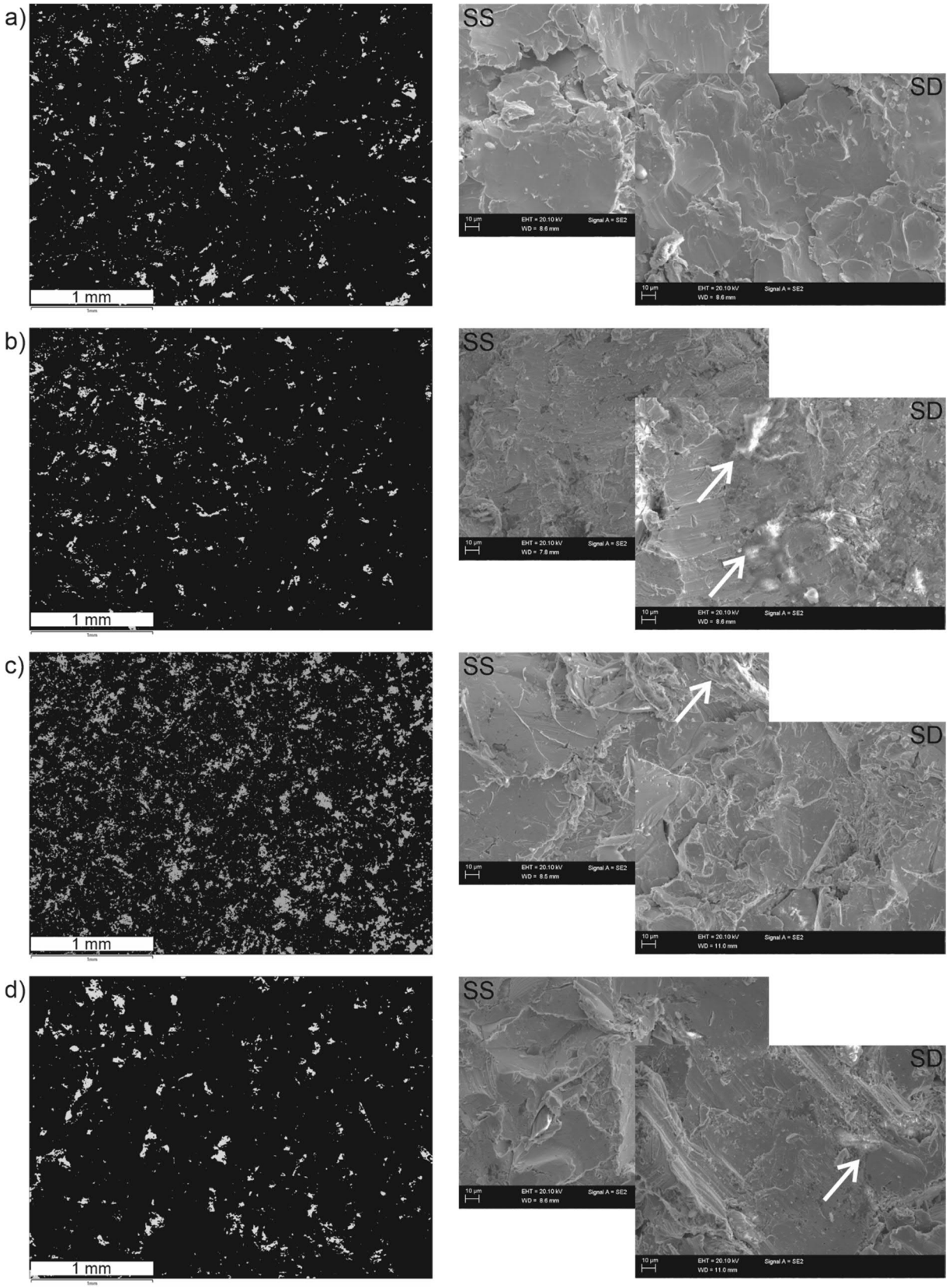

3

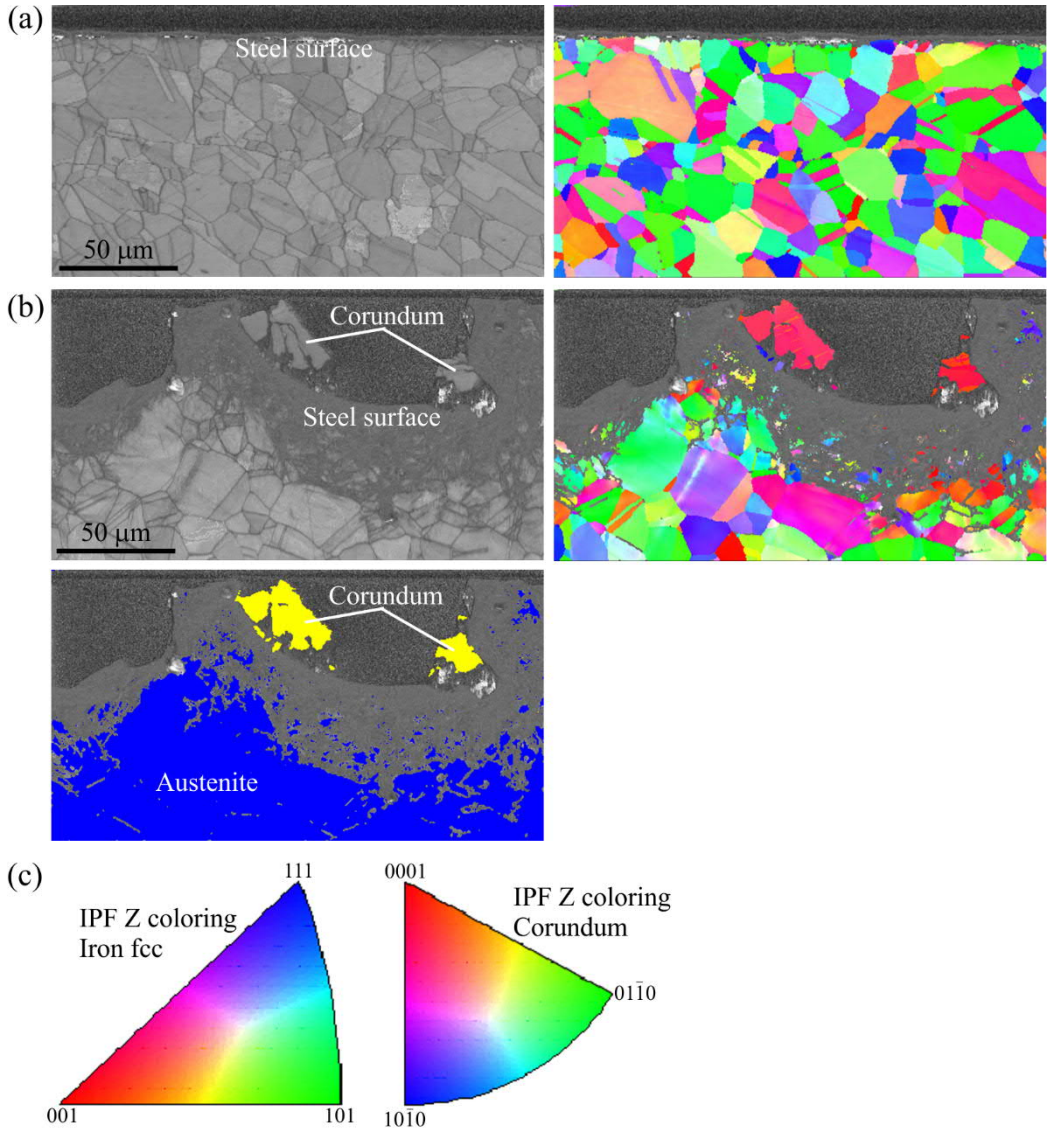
(a)
Steel surface
50 µm
(b)
Corundum
Steel surface
50 µm
Corundum
Austenite
(c)
111
IPF Z coloring
Iron fcc
001
101
0001
IPF Z coloring
Corundum
01$\bar{1}$0
10$\bar{1}$0

4

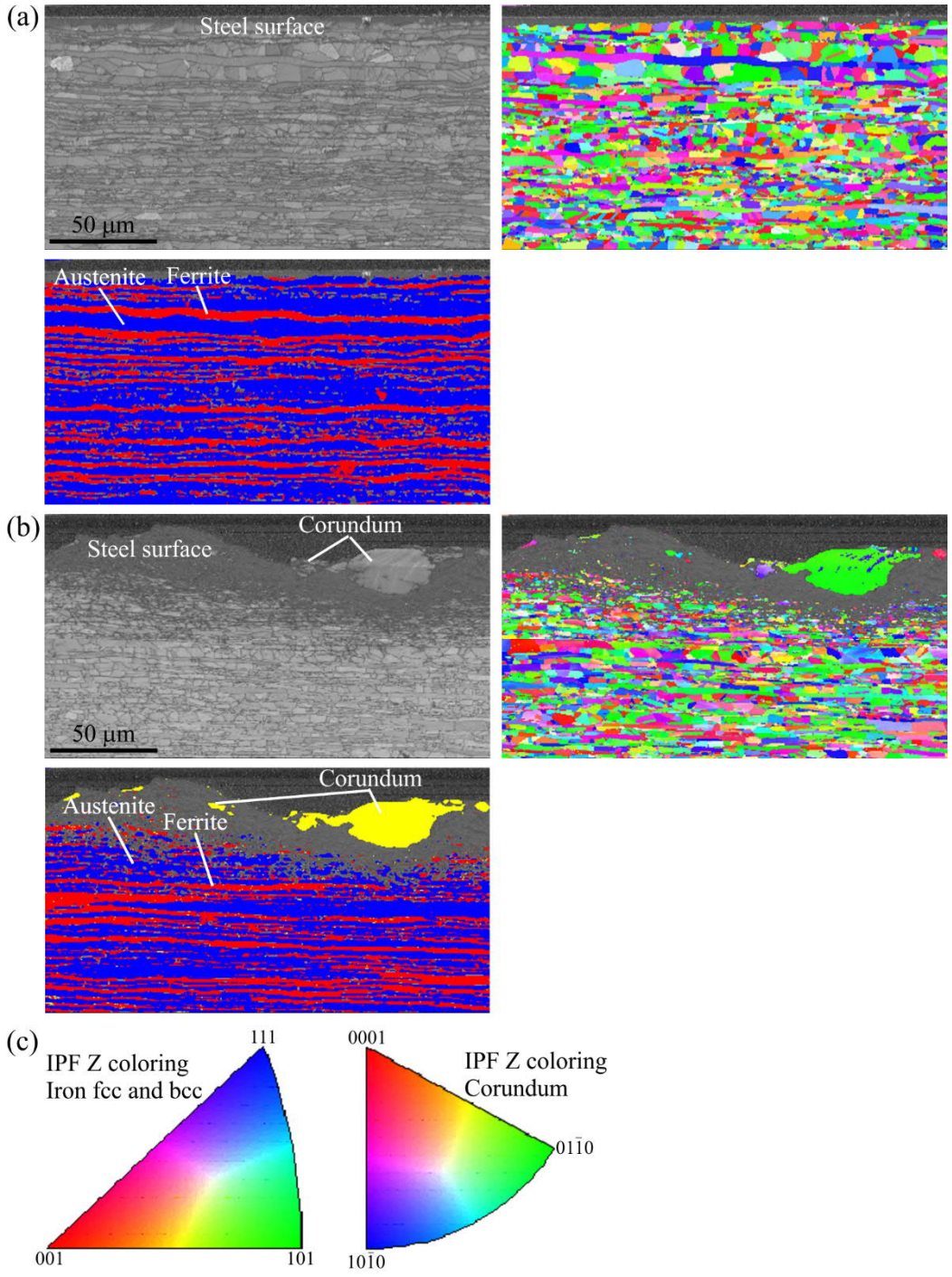
(a)
Steel surface
50 µm
Austenite
Ferrite
(b)
Steel surface
Corundum
50 µm
Corundum
Austenite
Ferrite
(c)
IPF Z coloring
Iron fcc and bcc
111
001
101
0001
IPF Z coloring
Corundum
01$\bar{1}$0
10$\bar{1}$0

5

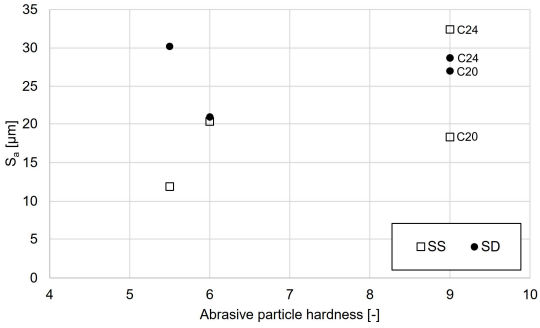
35
30
25
20
15
10
5
0
S_a [µm]
4
5
6
7
8
9
10
Abrasive particle hardness [-]
C24
C24
C20
C20
SS
SD

a)

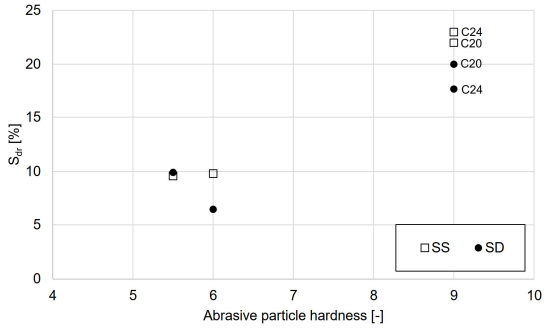
25
20
15
10
5
0
S_{dr} [%]
4
5
6
7
8
9
10
Abrasive particle hardness [-]
C24
C20
C20
C24
SS
SD

b)

6

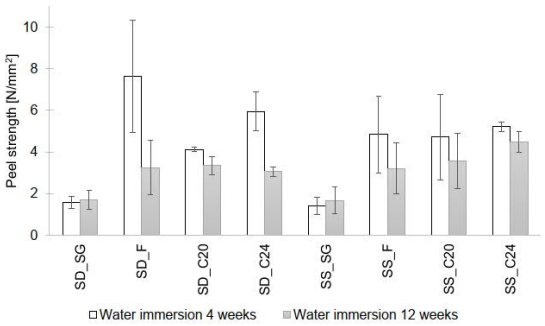
Peel strength [N/mm²]
10
8
6
4
2
0
SD_SG
SD_F
SD_C20
SD_C24
SS_SG
SS_F
SS_C20
SS_C24
Water immersion 4 weeks
Water immersion 12 weeks

a)

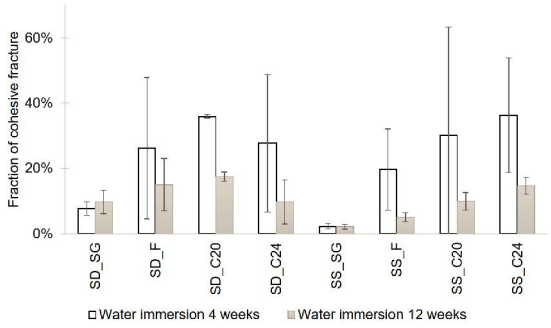
Fraction of cohesive fracture
60%
40%
20%
0%
SD_SG
SD_F
SD_C20
SD_C24
SS_SG
SS_F
SS_C20
SS_C24
Water immersion 4 weeks
Water immersion 12 weeks

b)

7

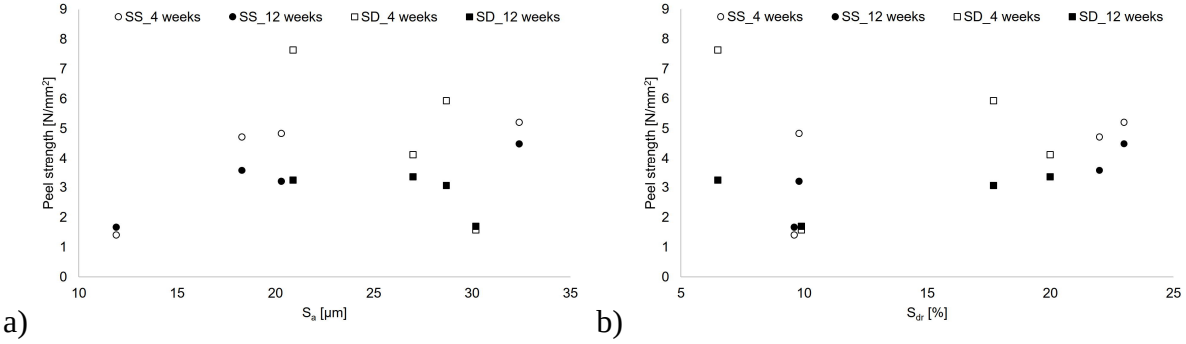
SS_4 weeks
SS_12 weeks
SD_4 weeks
SD_12 weeks
Peel strength [N/mm²]
S_a [µm]
S_{dr} [%]

a) b)

8

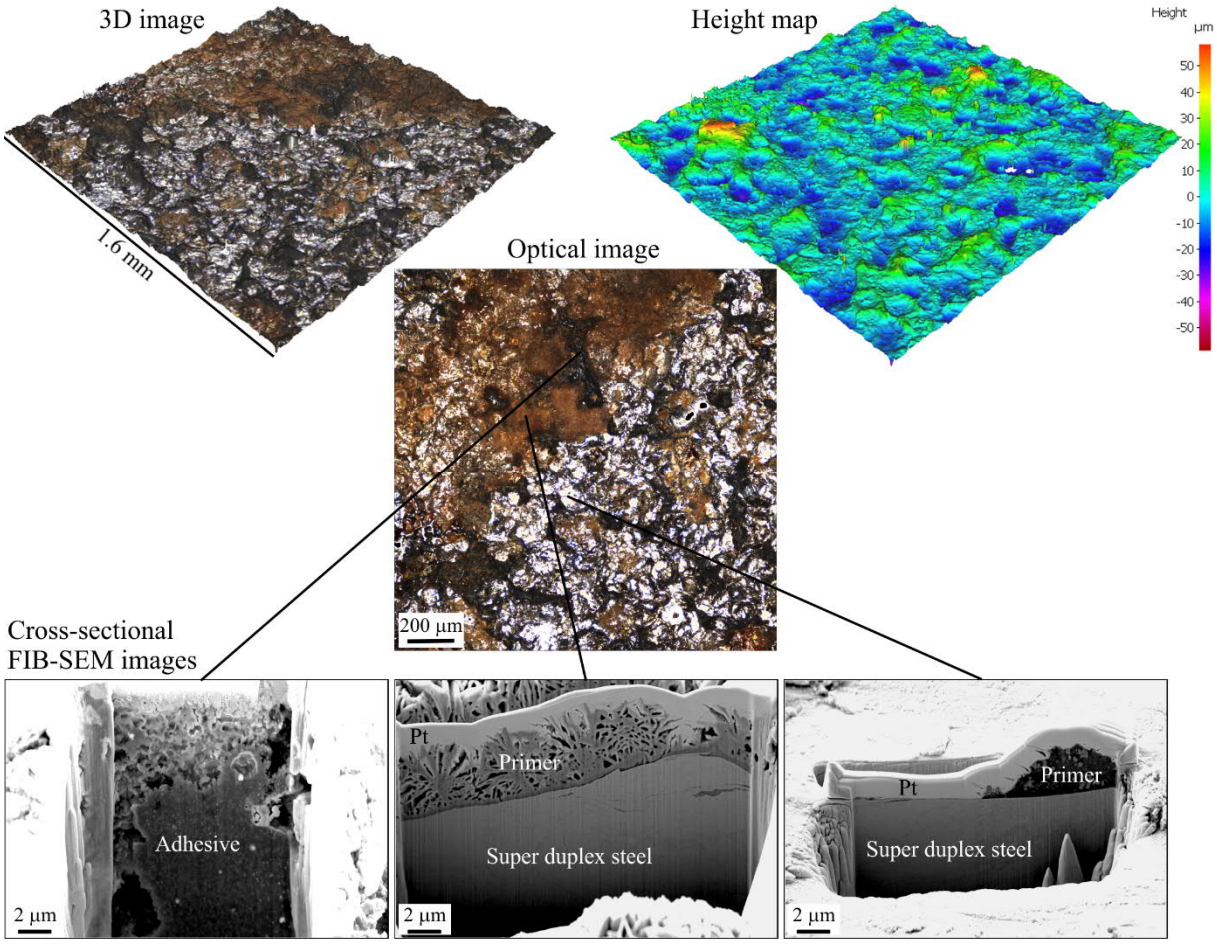
3D image
1.6 mm
Height map
Height
µm
50
40
30
20
10
0
-10
-20
-30
-40
-50
Optical image
200 µm
Cross-sectional
FIB-SEM images
Adhesive
2 µm
Pt
Primer
Super duplex steel
2 µm
Pt
Primer
Super duplex steel
2 µm

9